

# Band discontinuities at Si-TCO interfaces from quasiparticle calculations: Comparison of two alignment approaches

B. Höffling,\* A. Schleife, C. Rödl, and F. Bechstedt

*Institut für Festkörperteorie und -optik, Friedrich-Schiller-Universität, Max-Wien-Platz 1, D-07743 Jena, Germany and European Theoretical Spectroscopy Facility (ETSF)*

(Received 25 August 2011; revised manuscript received 5 December 2011; published 6 January 2012)

Modern quasiparticle theory based on hybrid functionals and the *GW* approximation yields electronic band structures with a high accuracy for silicon but also for oxides applied as transparent electrodes or layers in solar cells. The quasiparticle electronic structures are used to derive natural band discontinuities applying two different methods, a modified Tersoff method for the branch-point energy and the Shockley-Anderson model via the electron affinity rule. For the known Si-SiO<sub>2</sub> interface, which leads to type-I junctions, we demonstrate that both approaches are in good agreement with measured values. For the Si-oxide heterojunctions we observe a tendency for misaligned type-II heterostructures for In<sub>2</sub>O<sub>3</sub>, ZnO, and SnO<sub>2</sub>, which indicates highly efficient separation of electron-hole pairs generated in the Si layer. We show how surface orientation and structure as well as many-body effects influence the ionization energy and electron affinity and, hence, the band discontinuities obtained within the Shockley-Anderson model.

DOI: [10.1103/PhysRevB.85.035305](https://doi.org/10.1103/PhysRevB.85.035305)

PACS number(s): 73.20.At, 71.20.-b, 73.30.+y, 73.40.Lq

## I. INTRODUCTION

Transparent conducting oxides (TCOs) such as In<sub>2</sub>O<sub>3</sub>, SnO<sub>2</sub>, and ZnO are important materials with applications as transparent electrodes in optoelectronic or photovoltaic devices and sensors.<sup>1</sup> They are known to be transparent not only in the visible spectral region of about 400 to 700 nm but almost in the entire range of the solar spectrum and usually exhibit a high electron conductivity.<sup>2–4</sup> Recently, even the possibility of transparent electronics based on doped oxides has been suggested.<sup>5,6</sup> Such oxides are also used in silicon (Si) photonics and Si-based solar cells, sometimes together with extremely thin insulating SiO<sub>2</sub> layers.<sup>7</sup> Therefore, knowledge about the interfaces of TCOs with crystalline Si layers is extremely important but poor in praxis. This holds especially for the energy-band alignment of heterostructures of such oxides with silicon.<sup>8,9</sup> The band discontinuities are virtually unknown. Direct measurements of the band discontinuities have not yet been published. Only band offsets of the ZnO-Si interface have been estimated using measured electron affinity and work function of Si and ZnO. They indicate a type-II heterosystem.<sup>10–12</sup>

Natural band discontinuities can be derived if electronic properties of the two materials, semiconductors and/or insulators, on both sides of the interface are known. The highly important energy-band diagram near the interface can be constructed if the electron affinities  $A$  and the ionization energies  $I$  are known as energy distances to the vacuum level. In the spirit of the Shockley model for metal-semiconductor contacts<sup>13,14</sup> Anderson<sup>15</sup> made the first attempt to explain band offsets by alignment of the vacuum levels of the two nonmetals in contact. This method does not take into account electronic effects of the actual interface and, therefore, rests on the assumption that interface states do not play an important role. While  $A$  and  $I$  for silicon are well known and more or less accepted,<sup>14,16</sup> the situation is completely different for the TCOs. Available experimental values for  $I$  vary with the preparation technique of the oxide layers, the postdeposition

treatment, and the doping (see, e.g., Ref. 17). Since even the fundamental gaps

$$E_g = I - A \quad (1)$$

are under discussion for In<sub>2</sub>O<sub>3</sub> and SnO<sub>2</sub> (see Refs. 18–20 and references therein), the resulting electron affinities  $A$  are questionable. As a consequence, electronic-structure parameters of the TCOs, such as  $I$  and  $A$ , are controversially discussed in the literature.<sup>21–26</sup>

A completely different alignment concept is based on the charge neutrality level or branch-point (BP) energy  $E_{BP}$ . The use of such a universal reference level has been suggested by Frenslley and Kroemer.<sup>27</sup> This concept is based on the influence of interface states (or surface states for the semiconductor-vacuum interface) in the fundamental gap. It goes back to the idea of virtual gap states (ViGSs) derived from the complex bulk band structure.<sup>16,28–31</sup> The branch-point concept of Tersoff,<sup>32</sup> which is very similar to an earlier approach of Tejedor and Flores,<sup>33</sup> is easily accessible from a physical point of view. The branch-point energies of the nonmetals in contact determine the band lineup. Nevertheless, the theoretical determination of the branch-point energy asks for some approximations.<sup>30,32,34</sup> However, the experimental results concerning the branch-point position with respect to the band edges are also under debate. Different conclusions have been published with respect to the occurrence of surface electron accumulation<sup>35,36</sup> or surface electron depletion.<sup>21,37</sup> Nevertheless, in contrast to the majority of semiconductors and insulators there are strong theoretical and experimental arguments<sup>34–36,38</sup> that the branch points of In<sub>2</sub>O<sub>3</sub>, SnO<sub>2</sub>, and ZnO lie in the lowest conduction band and not in the fundamental gap.

A more direct determination of the band lineup is possible by means of an explicit self-consistent interface calculation. This has been done in the past for lattice-constant and crystal-structure matched semiconductors (see, e.g., Refs. 39 and 40). However, for the Si-TCO systems such calculations are at

or beyond the limits of current computational possibilities. The adjacent crystals possess different crystal structures, lattice constants, and completely different chemical bonding. A construction of a reasonable atomic geometry of even a strained interface is extremely difficult.

The difficulties to investigate Si-oxide heterojunctions experimentally arise mainly from sample quality and sample preparation problems. Theoretical methods like *ab initio* calculations do not face those difficulties and can help to advance the understanding of these important interfaces. The application of modern quasiparticle (QP) band-structure theory<sup>41,42</sup> allows us to compute characteristic energies and band discontinuities<sup>34</sup> with high precision. Indeed, the QP band-structure theory has now reached an accuracy, which allows us to treat oxides, whose electronic properties are notoriously difficult to predict.<sup>18,20,42,43</sup>

In the present paper, the QP band structures are used to compute ionization energies, electron affinities, and branch-point energies for  $\text{In}_2\text{O}_3$ ,  $\text{SnO}_2$ , and  $\text{ZnO}$ . Applying two different alignment procedures the conduction- and valence-band discontinuities  $\Delta E_c$  and  $\Delta E_v$  are computed with respect to crystalline silicon using the branch-point energies or the vacuum levels. The underlying theoretical and computational methods are presented in Sec. II. In Sec. III the two alignment methods to derive band discontinuities are discussed and compared for the well-studied model Si-SiO<sub>2</sub> interface. Next we present ionization energies, electron affinities, and branch-point energies for the TCOs and discuss their reliability in the light of available measured values (Sec. IV). These results are used to predict band discontinuities and, hence, band lineups for the junctions with crystalline silicon. Finally, in Sec. V we conclude with a brief summary.

## II. COMPUTATIONAL METHODS

### A. Atomic geometry

The ground-state properties of the oxides are computed in the framework of the density functional theory (DFT)<sup>44</sup> using the local density approximation (LDA)<sup>45</sup> for exchange and correlation (XC). Explicitly, we use the XC functional of Ceperley and Alder.<sup>46</sup> The  $\text{ZnO}$  ground-state properties have been computed in the generalized gradient approximation (GGA), using the PW91 functional to model XC.<sup>47</sup> All computations are performed using the Vienna *Ab initio* Simulation Package (VASP).<sup>48</sup> The electronic wave functions are expanded using plane waves up to kinetic energies of 450 (Si), 500 ( $\text{SiO}_2$ ), 550 ( $\text{In}_2\text{O}_3$ ), 450 ( $\text{SnO}_2$ ), and 500 eV ( $\text{ZnO}$ ), respectively.<sup>18,20,41–43</sup> The projector-augmented wave (PAW) method<sup>49</sup> is used to describe the electron-ion interaction in the core region. Usually it allows for the accurate treatment of first-row elements such as oxygen and localized semicore states such as  $\text{In}4d$ ,  $\text{Zn}3d$ , and  $\text{Sn}4d$  by modest plane-wave cutoffs.

Silicon crystallizes in the cubic diamond (*cd*) structure. In the case of  $\text{In}_2\text{O}_3$  we study the two most stable polymorphs, the rhombohedral (*rh*) and the body centered cubic (*bcc*) bixbyite geometries, while for  $\text{SnO}_2$  only the most favored rutile (*rt*) geometry is investigated. For the purpose of comparison also the native oxide of silicon,  $\text{SiO}_2$ , is studied within

TABLE I. Lattice constants (in Å) obtained within DFT-LDA (GGA for  $\text{ZnO}$ ) for the oxides and silicon. For the cubic materials only the cubic lattice constant  $a_0$  is given while for the noncubic oxides,  $a$ ,  $c$ , and  $c/a$  are listed. Values in parentheses are from experiment.<sup>52–55</sup>

| Material                             | Lattice constant                             |  |  |
|--------------------------------------|--|--|--|
|                                      | $a_0, a$                                     | $c$  | $c/a$                                      |
| <i>cd</i> -Si                        | 5.402 <sup>a</sup><br>(5.431) <sup>b</sup>   |  |  |
| <i>cb</i> - $\text{SiO}_2$           | 7.391 <sup>b</sup><br>(7.131) <sup>d</sup>   |  |  |
| <i>bcc</i> - $\text{In}_2\text{O}_3$ | 10.094 <sup>e</sup><br>(10.117) <sup>f</sup> |  |  |
| <i>rh</i> - $\text{In}_2\text{O}_3$  | 5.479 <sup>e</sup><br>(5.487) <sup>f</sup>   | 14.415 <sup>e</sup><br>(14.510) <sup>f</sup> | 2.631 <sup>e</sup><br>(2.644) <sup>f</sup> |
| <i>rt</i> - $\text{SnO}_2$           | 4.737 <sup>g</sup><br>(4.737) <sup>h</sup>   | 3.200 <sup>g</sup><br>(3.186) <sup>h</sup>   | 0.676 <sup>g</sup><br>(0.673) <sup>h</sup> |
| <i>wz</i> - $\text{ZnO}$             | 3.28 <sup>i</sup><br>(3.249) <sup>b</sup>    | 5.28 <sup>i</sup><br>(5.204) <sup>b</sup>    | 1.61 <sup>i</sup><br>(1.602) <sup>b</sup>  |

<sup>a</sup>Reference 41.

<sup>b</sup>Reference 52.

<sup>c</sup>Reference 56.

<sup>d</sup>Reference 53.

<sup>e</sup>Reference 18.

<sup>f</sup>Reference 54.

<sup>g</sup>Reference 20.

<sup>h</sup>Reference 55.

<sup>i</sup>Reference 57.

the cubic  $\beta$ -cristobalite (*cb*) structure with an *fcc* Bravais lattice, whose electronic properties are similar to amorphous  $\text{SiO}_2$ .<sup>50</sup> The Brillouin-zone (BZ) integrations are performed by summations over special points of the Monkhorst-Pack (MP) type.<sup>51</sup> Monkhorst-Pack meshes of  $5 \times 5 \times 5$  (cubic) or  $8 \times 8 \times 8$  (rhombohedral)  $k$  points are found to be sufficient for  $\text{In}_2\text{O}_3$ .<sup>18</sup> For hexagonal  $\text{ZnO}$  a  $12 \times 12 \times 7$  mesh is applied.<sup>42</sup> In the *rt*- $\text{SnO}_2$  case, we use a mesh of  $8 \times 8 \times 14$   $k$  points.<sup>20</sup> Finally, meshes of  $8 \times 8 \times 8$  and  $16 \times 16 \times 16$   $k$  points have been applied for *cb*- $\text{SiO}_2$  and *cd*-Si, respectively.

The minimization of the DFT-LDA total energy leads to the cubic ( $a_0$ ) and noncubic ( $a$ ,  $c$ ) lattice constants in Table I, previously presented in Refs. 18,20,41,56, and 57. They are in good agreement with experimental data. The significant deviation from the measured value of the  $\text{SiO}_2$  lattice constant is due to the fact that the measurements were carried out on the  $I\bar{4}2d$  geometry while we use the ideal structure with the  $Fd\bar{3}m$  space group. Our lattice constant is in good agreement with other theoretical predictions for this geometry.<sup>53</sup> Apart from  $c$  of *rt*- $\text{SnO}_2$  the lattice constants differ from the corresponding experimental values by less than 1%. The obtained atomic geometries are used for the electronic structure calculations and as stacking geometries for the surface simulations.

The surface calculations are carried out using the repeated slab supercell method. The slabs consist of 9, 11, 8, 19, and 20 layers for *bcc*- $\text{In}_2\text{O}_3(001)$ , *rh*- $\text{In}_2\text{O}_3(001)$ , *rt*- $\text{SnO}_2(001)$ , *rt*- $\text{SnO}_2(100)$ , and *wz*- $\text{ZnO}(001)$ , respectively, with 12 Å of vacuum each. Usually orthorhombic slabs are applied resulting typically in  $N \times N \times 1$  MP meshes, with  $N = 3, 8, 8$ , and 12 for

*bcc*-In<sub>2</sub>O<sub>3</sub>, *rh*-In<sub>2</sub>O<sub>3</sub>, SnO<sub>2</sub>(001), and ZnO, respectively. For the SnO<sub>2</sub>(100) slab we used an MP mesh of  $8 \times 14 \times 1$ .

### B. Quasiparticle band structures

The resulting structural parameters are used for the calculation of excited-state properties, more precisely the QP band structures.<sup>41,58</sup> The QP equation with a self-energy in Hedin's *GW* approximation is solved perturbatively on top of the self-consistent solution of a generalized Kohn-Sham (gKS) equation. In the zeroth approximation the *GW* self-energy is expressed by the spatially nonlocal XC potential  $V_{XC}(\mathbf{x}, \mathbf{x}')$  using the hybrid functional HSE of Heyd, Scuseria, and Ernzerhof<sup>59–62</sup> [employing a screening parameter of  $\omega = 0.15$  a.u.<sup>-1</sup> instead of  $\omega = 0.11$  a.u.<sup>-1</sup> (see disambiguation in Ref. 63)]. In a first iteration the QP wave functions remain unchanged and are replaced by the solutions of the gKS equation with the potential  $V_{XC}(\mathbf{x}, \mathbf{x}')$ . The QP shifts for the gKS eigenvalues are computed within the  $G_0W_0$  approach.<sup>64</sup> It has been demonstrated that for the compounds investigated in this work this treatment leads to energy gaps in excellent agreement with measured values.<sup>18,20,41,42,65</sup>

### C. Electrostatic potentials

Most important for the absolute positions of the electronic energy levels in solids is the electrostatic potential  $V(\mathbf{x})$  acting on the electrons. It can be derived from the effective single-particle potential occurring in the Kohn-Sham equation<sup>45</sup> or the generalized Kohn-Sham equation.<sup>41</sup> It is defined as the local part of the electron-ion interaction represented by the pseudopotentials and the Hartree potential of the electrons. This holds independently of the local (LDA), semilocal (GGA), or nonlocal (HSE) description of the exchange-correlation part of the effective single-particle potential. The electrostatic potential obtained within the HSE approach is also used for describing the QP case, since the wave functions and, hence, the electron density are not changed during the first-order perturbation step. The only variation of the electrostatic potentials between LDA/GGA and HSE is due to the change of the electron density resulting from the use of different XC functionals. However, this effect is only locally important if localized states (such as semicore *d* states) contribute to the density of the valence electrons.

As an example, the electrostatic potentials obtained for bulk *bcc*-In<sub>2</sub>O<sub>3</sub> in LDA and HSE are plotted in Fig. 1 along a cubic axis. For practical reasons only an average potential  $\tilde{V}(z)$  over a plane perpendicular to the studied normal direction of a surface or interface, assumed to be the *z* axis, is given. The details of the electron density modified by the local or nonlocal XC potential influence the electrostatic potentials only close to the atomic cores due to the strong localization of the In4*d* and O2*s* states. However, these modifications are only of local importance and can be neglected if the potential is averaged also over the *z* direction within the slab. Therefore, the DFT-LDA potentials are used below for the band alignment between bulk and surface of the semiconductors. The strongest influence of the XC potential is visible for the positions of the conduction-band minimum (CBM)  $E_c$  and valence-band maximum (VBM)  $E_v$  relative to the potentials. After inclusion

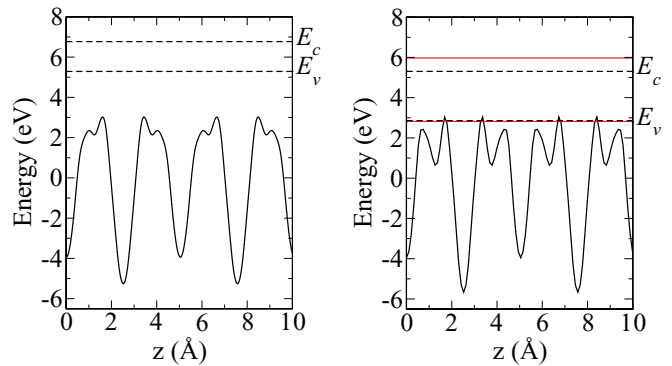


FIG. 1. (Color online) Electrostatic potential  $\tilde{V}(z)$  averaged over planes perpendicular to the cubic axis  $z \parallel [001]$  for bixbyite In<sub>2</sub>O<sub>3</sub>. The results obtained within (a) LDA and (b) HSE descriptions of the electron density are plotted. In addition, the corresponding positions of the valence-band maximum  $E_v$  and conduction-band minimum  $E_c$  are given as dashed horizontal lines. In (b) the band edges including QP effects are shown as red solid lines.

of the QP corrections we obtain the position of the QP band edges relative to the electrostatic potential. In Fig. 1 the LDA Kohn-Sham values  $E_c$  and  $E_v$  [Fig. 1(a)] as well as the HSE and the QP energies  $E_c$  and  $E_v$  [Fig. 1(b)] are given. The comparison of the two panels shows that the XC functional and QP effects drastically influence the position of the band edges with respect to the electrostatic potential. The application of a nonlocal potential shifts both band edges downward by several eV and opens up the gap. The *GW* QP corrections lead to a very small downward shift of  $E_v$  and a considerable upward shift of  $E_c$ , which widens the gap even further.

## III. BAND ALIGNMENT AT THE HETEROINTERFACE

### A. General considerations

The fundamental parameters determining many physical properties of heterostructures of nonmetals are the relative positions  $E_v$  and  $E_c$  of the QP valence and conduction-band extrema at the interface of the two materials 1 and 2. The band discontinuities or band (edge) offsets are defined as

$$\Delta E_c = E_{c2} - E_{c1}, \quad \Delta E_v = E_{v1} - E_{v2} \quad (2)$$

with  $\Delta E_c + \Delta E_v = E_{g2} - E_{g1} = \Delta E_g$ , the band-gap difference of the semiconductors in contact. The definition of the signs of the band discontinuities  $\Delta E_v$  and  $\Delta E_c$  is chosen in such a way that the oxide with the wider gap forms a straddling type-I heterostructure<sup>14</sup> with silicon if  $\Delta E_v > 0$  and  $\Delta E_c > 0$ .

In the introduction two approaches for calculating natural-band discontinuities using two different alignment procedures<sup>15,27</sup> have been outlined. In many cases these approaches may give results that reasonably describe the transition of the electronic properties at the interface.<sup>14,16,31</sup> However, the actual preparation of the interface also influences such a heterotransition. Therefore, especially for heterovalent, heterocrystalline, and nonlattice matched crystals, theoretical and experimental data for the band offsets are at variance.

For pseudomorphic interfaces with a more or less defined atomic geometry and stoichiometry, there exists a well-defined procedure to compute the band discontinuities  $\Delta E_v$  and

$\Delta E_c$  at the interface applying *ab initio* electronic-structure calculations.<sup>66,67</sup> One artificially introduces a periodicity into the problem by constructing a supercell consisting of two slabs of the respective semiconductors in a particular orientation. If possible (e.g., for nonpolar interfaces) the two interfaces should be equivalent in geometry and stoichiometry to avoid artificial dipole potentials and unphysical charge transfer. The electronic structure of the system is then calculated self-consistently. The planar average of the electrostatic (or even the total) potential can then be plotted as shown for a bulk system in Fig. 1. Typically, the atomic oscillations within the material slabs are bulklike. Aligning these oscillations with the oscillations of the potential derived from the bulk calculations and taking into account the positions of  $E_v$  and  $E_c$  relative to these oscillations, one can derive the differences  $\Delta E_v$  and  $\Delta E_c$  of the absolute positions of the bulk bands on the two sides of the interface. Such a procedure can be further refined by self-consistent treatments. One of the most important quantities is the overall interface dipole that can be made self-consistent by itself and already provides good results even if the potential shape is not fully made self-consistent.<sup>40</sup>

Unfortunately, the interfaces of the transparent conducting oxides under consideration with other semiconductors (e.g., Si) are usually much more complex and more difficult to treat theoretically than well-defined atomic interface geometries. Usually the atomic basis in a primitive unit cell of the bulk crystal contains more than two atoms. For instance, bixbyite  $\text{In}_2\text{O}_3$  possesses an atomic basis with 40 atoms. The chemical bonds are rather ionic. The oxygen atoms tend to be twofold negatively charged ions.<sup>18</sup> Consequently, besides the fourfold coordination in ZnO also higher coordinations of the metal atoms appear. Less directional but strong electrostatic forces play a role for the interface formation. Moreover, the atomic structures of the oxides and Si do not lead to pseudomorphic interfaces. Already the description of a (001) interface between  $\beta$ -cristobalite  $\text{SiO}_2$  and diamond Si requires model assumptions about stoichiometry, dangling bond passivation, interface dipoles, and strain in the oxide.<sup>68</sup>

Despite the fact that the heterointerfaces silicon-TCO with  $\text{In}_2\text{O}_3$ ,  $\text{SnO}_2$ , or ZnO on the oxide side play an important role for the action of numerous devices (e.g., for the separation of optically excited electrons and holes in the silicon absorber of a Si-based solar cell) practically nothing is known about these interfaces from a microscopic point of view. For that reason we have to resort to the natural-band discontinuities  $\Delta E_c$  and  $\Delta E_v$ .

### B. Band alignment via branch points

The QP band structures allow the computation of the branch-point energies  $E_{\text{BP}}$  using a recently developed approximative method.<sup>34</sup> It is based on a modification of the Tersoff method,<sup>32</sup> which relies solely on bulk properties.<sup>30,33,69,70</sup> In practice, the branch-point energy is computed as a BZ average of the QP eigenvalues of the lowest  $N_{\text{CB}}$  conduction bands and the highest  $N_{\text{VB}} = 2N_{\text{CB}}$  valence bands

$$E_{\text{BP}} = \frac{1}{2N_{\mathbf{k}}} \sum_{\mathbf{k}} \left[ \frac{1}{N_{\text{CB}}} \sum_i^{N_{\text{CB}}} \varepsilon_{c_i}(\mathbf{k}) + \frac{1}{N_{\text{VB}}} \sum_j^{N_{\text{VB}}} \varepsilon_{v_j}(\mathbf{k}) \right] \quad (3)$$

The number of bands is scaled with the number of valence electrons (without  $d$  electrons). For crystals with two atoms in the primitive unit cell (e.g.,  $cd$ -Si) it holds that  $N_{\text{CB}} = 1$ . Correspondingly, one obtains  $N_{\text{CB}} = 2$  ( $wz$ -ZnO, 4 atoms), 2 ( $cb$ - $\text{SiO}_2$ , 3 atoms), 4 ( $rt$ - $\text{SnO}_2$ , 6 atoms), 6 ( $rh$ - $\text{In}_2\text{O}_3$ , 10 atoms), and 12 ( $bcc$ - $\text{In}_2\text{O}_3$ , 40 atoms).

Neglecting the real structure of an interface including interface dipole, stoichiometry, and interdiffusion, the branch-point energies  $E_{\text{BP}}$  can be used to derive the natural-band discontinuities. With the VBM  $E_v = 0$  as energy zero, the CBM  $E_c$  takes the value of  $E_g$ . Using  $E_{\text{BP}}$  and  $E_g$  as listed in Table II the band offsets are calculated as

$$\begin{aligned} \Delta E_c &= [E_g(\text{oxide}) - E_{\text{BP}}(\text{oxide})] - [E_g(\text{Si}) - E_{\text{BP}}(\text{Si})], \\ \Delta E_v &= E_{\text{BP}}(\text{oxide}) - E_{\text{BP}}(\text{Si}). \end{aligned} \quad (4)$$

The branch-point energy is used as universal reference level to align the energy bands of Si and the TCO according to Frenslay and Kroemer.<sup>27</sup> The physical model behind this assumes the existence of interface-induced virtual gap states, which are donorlike above and acceptorlike below  $E_{\text{BP}}$ . That is why the branch-point energy pins the Fermi level at the interface and can be used as a universal reference energy. The positions of the band extrema  $E_v$  and  $E_c$  relative to the reference level can be interpreted as natural-band discontinuities.<sup>71,72</sup> The approximation in the branch-point alignment method consists in the neglect of the influence of native surface dipoles and interface orientation. The resulting band discontinuities are listed in Table III.

### C. Band alignment via vacuum levels

Since for Si-TCO interfaces reliable models, which allow a direct computation of band offsets do not exist, we suggest to do an intermediate step by studying the materials surfaces or vacuum-oxide interfaces. For an idealized surface this allows the description of the surface barriers and, consequently, the determination of the absolute positions of the band edges  $E_v$  and  $E_c$  with respect to the vacuum level  $E_{\text{vac}}$  in the QP approach. The energy differences

$$I = E_{\text{vac}} - E_v, \quad A = E_{\text{vac}} - E_c \quad (5)$$

define the ionization energy  $I$  and the electron affinity  $A$  for such a surface. Within this idealized frame the two quantities are directly related to the fundamental QP gap by<sup>73</sup>

$$E_g = I - A = E_c - E_v. \quad (6)$$

Results are graphically presented in Fig. 2 for the case of the Si- $\text{SiO}_2$  interface. They clearly show that in a certain distance from the surface the electrostatic potentials exhibit a bulklike behavior. Within the surface region there is a steep increase to a plateau which represents the vacuum level  $E_{\text{vac}}$ .

The calculated ionization energies  $I$  and electron affinities  $A$  (cf. Table II) can also be used to derive natural-band discontinuities in the framework of the electron affinity rule<sup>15</sup> or, more general, the Shockley-Anderson model<sup>14,74</sup>

$$\Delta E_c = A(\text{Si}) - A(\text{oxide}), \quad \Delta E_v = I(\text{oxide}) - I(\text{Si}). \quad (7)$$

In principle, this model employs the vacuum level  $E_{\text{vac}}$  according to definition (5) as universal reference level for the

TABLE II. Characteristic energies: fundamental gap  $E_g$ , branch-point energy  $E_{BP}$ , electron affinity  $A$ , and ionization energy  $I$  of transparent conducting oxides derived from QP calculations. For comparison, the data for Si and SiO<sub>2</sub> are listed too. All values in eV. The surface orientation used for the calculation of  $I$  and  $A$  is indicated by the Miller indices ( $hkl$ ) or ( $hkil$ ). Experimental values are given in parentheses.

| Crystal                                    | Orientation | $E_g$                       | $E_{BP}$                                 | $A$   | $I$   |
|--|-------------|-----------------------------|--|---|---|
| <i>cd</i> -Si                              | (001)       | 1.29<br>(1.17) <sup>a</sup> | 0.29<br>(0.36) <sup>b</sup>              | 4.54<br>(4.0–4.2) <sup>d</sup>                            | 5.83<br>(5.15–5.33) <sup>d</sup>                          |
| <i>cb</i> -SiO <sub>2</sub>                | (001)       | 8.76<br>(8.9) <sup>c</sup>  | 4.52<br>(4.9) <sup>b</sup>               | 1.44  | 10.20   |
| <i>rh</i> -In <sub>2</sub> O <sub>3</sub>  | (0001)      | 3.31<br>(3.02) <sup>e</sup> | 3.79<br>(3.50) <sup>e</sup>              | 6.11  | 9.41  |
| <i>bcc</i> -In <sub>2</sub> O <sub>3</sub> | (001)       | 3.15<br>(2.93) <sup>e</sup> | 3.50<br>(3.58) <sup>e</sup>              | 5.95<br>(3.5–5.0) <sup>f</sup>                            | 9.10<br>(7.1–8.6) <sup>f</sup>                            |
| <i>rt</i> -SnO <sub>2</sub>                | (100)       | 3.64<br>(3.6) <sup>g</sup>  | 3.82                                     | 4.10<br>(4.44) <sup>h</sup>                               | 7.73<br>(8.04) <sup>h</sup>                               |
|  | (001)       |                             |  | 3.45<br>(4.44) <sup>h</sup>                               | 7.08<br>(8.04) <sup>h</sup>                               |
| <i>wz</i> -ZnO                             | (0001)      | 3.21<br>(3.38) <sup>a</sup> | 3.40<br>(3.6, 3.04, 3.78) <sup>i,j</sup> | 5.07<br>(4.05, 3.7–4.6,<br>4.42, 4.64) <sup>d,h,k,l</sup> | 8.24<br>(7.45, 7.1–8.0,<br>7.82, 8.04) <sup>d,h,k,l</sup> |

<sup>a</sup>Reference 52.

<sup>b</sup>Reference 31.

<sup>c</sup>Reference 77.

<sup>d</sup>Reference 16.

<sup>e</sup>References 19 and 86.

<sup>f</sup>References 21 and 26.

<sup>g</sup>Reference 80.

<sup>h</sup>References 23 and 88.

<sup>i</sup>Reference 22.

<sup>j</sup>Reference 36.

<sup>k</sup>Reference 87.

<sup>l</sup>Reference 89.

band alignment. The band discontinuities (7) derived from the  $I$  and  $A$  values in Table II are listed in Table III.

The vacuum level alignment relies on several approximations that might limit its predictive power for band discontinuities. First, the model assumes the dipole at the interface to be the sum of the two surface dipoles (i.e., it neglects any charge transfer or charge rearrangements at

the interface). Furthermore, in computing  $I$  and  $A$  using the described method we encounter a theoretical problem in the QP description within Hedin's  $GW$  approximation for the full XC self-energy  $\Sigma = GW\Gamma$ , namely the neglect of vertex corrections by replacing the vertex function by  $\Gamma \equiv 1$ . It has been shown that the inclusion of vertex corrections in the QP calculations by applying rough approximations for the

TABLE III. Natural-band discontinuities  $\Delta E_c$  and  $\Delta E_v$  [Eqs. (4) and (7)] of the studied oxides with respect to the band positions in crystalline silicon derived by two different alignment procedures (see text) in comparison to experimental data. All values in eV.

| Si heterojunction                          | Alignment via $E_{BP}$ |              | Alignment via electron affinity rule |              | Experiment                              |  |
|--|------------------------|--------------|--------------------------------------|--------------|---|--|
|  | $\Delta E_c$           | $\Delta E_v$ | $\Delta E_c$                         | $\Delta E_v$ | $\Delta E_c$                            | $\Delta E_v$                               |
| <i>cb</i> -SiO <sub>2</sub>                | 3.24                   | 4.23         | 3.10                                 | 4.37         | 3.4 <sup>a</sup> , 3.13 <sup>b</sup>    | 4.4 <sup>a</sup> , 4.3 – 4.61 <sup>b</sup> |
| <i>rh</i> -In <sub>2</sub> O <sub>3</sub>  | –1.48                  | 3.50         | –1.57                                | 3.58         | –                                       | –  |
| <i>bcc</i> -In <sub>2</sub> O <sub>3</sub> | –1.35                  | 3.23         | –1.42                                | 3.27         | –0.61 <sup>c</sup> , –0.85 <sup>d</sup> | 2.6 <sup>e</sup> , 2.85 <sup>d</sup>       |
| <i>rt</i> -SnO <sub>2</sub> (100)          | –1.19                  | 3.53         | 0.44                                 | 1.83         | –0.25 <sup>d</sup>                      | 2.75 <sup>d</sup>                          |
| <i>rt</i> -SnO <sub>2</sub> (001)          |                        |              | 1.09                                 | 1.25         |   |  |
| <i>wz</i> -ZnO                             | –1.17                  | 3.09         | –0.53                                | 2.34         | –0.4 <sup>e</sup>                       | 2.55 <sup>e</sup>                          |

<sup>a</sup>Reference 78.

<sup>b</sup>Reference 16.

<sup>c</sup>Reference 92.

<sup>d</sup>see text.

<sup>e</sup>Reference 12.

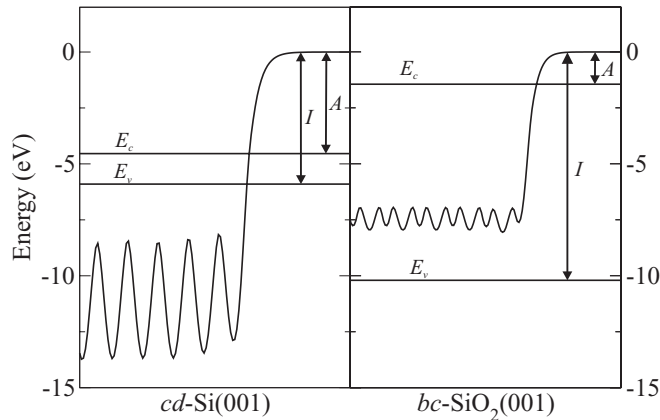


FIG. 2. Planar-averaged electrostatic potential near a surface for  $cd$ -Si(001) and  $cb$ -SiO<sub>2</sub>(001) computed within the LDA. The respective QP levels  $E_c$  and  $E_v$  are indicated by horizontal lines. Their difference yields the fundamental QP gaps  $E_g$ . The ionization energies  $I$  and electron affinities  $A$  are indicated. The vacuum level is used as zero of energy.

vertex function changes the position of the Si VBM only by 0.1 eV while the gap remains almost uninfluenced.<sup>75,76</sup> For SiO<sub>2</sub> the vertex corrections seem to have a somewhat stronger influence. They reduce  $I$  ( $A$ ) by about 0.6 (0.3) eV,<sup>76</sup> thereby closing the QP gap by the difference. So a variation of the band discontinuities of about 5–10 % due to further many-body effects cannot be excluded.

#### D. Test: Si-SiO<sub>2</sub> heterojunction

The gaps  $E_g$  as well as the branch-point energies  $E_{BP}$  of bulk silicon and SiO<sub>2</sub> in the  $\beta$ -cristobalite structure are listed in Table II. The QP gaps obtained within the HSE+ $G_0W_0$  approach are in reasonable agreement with experimental values.<sup>52,77</sup> The deviations are of the order of 0.1 eV which may be considered as the inaccuracy of the applied QP approach. The branch-point energy  $E_{BP} = 0.29$  eV resulting for Si from the QP band structure is almost in agreement with a measured value of 0.36 eV.<sup>31</sup> The deviation is smaller than 0.1 eV. In this case the branch point is situated closer to the VBM than to the CBM, as predicted by Tersoff.<sup>32</sup> For SiO<sub>2</sub> we find  $E_{BP}$  close to the midgap position, consistent with measurements.<sup>31</sup> The alignment of the branch points of Si and SiO<sub>2</sub> leads to a band lineup with natural-band discontinuities  $\Delta E_c = 3.24$  eV and  $\Delta E_v = 4.23$  eV (see Table III) in excellent agreement with measured data (see compilation in Refs. 16 and 78). The alignment via the vacuum level leads to similar values  $\Delta E_c = 3.10$  eV and  $\Delta E_v = 4.37$  eV (Table III). Deviations between the two alignment methods are of the order of or less than the deviations within the measured data.

This clearly positive conclusion with respect to the results of the two completely different methods and their agreement with experimental data for the band offsets suggest their applicability to the Si-TCO heterojunctions. Nevertheless, we have to mention again that real-structure effects like stoichiometry, dangling bond passivation, interface dipoles, and strain have been omitted. Furthermore, the interface orientation may play a role. Already for a silicon surface, the orientation and the accompanying morphology (atomic

arrangement due to relaxation and reconstruction) leads to a variation of about 0.55 eV for Si(001) or 0.22 eV for Si(111) for the ionization potential<sup>79</sup> and, hence, influence the band offsets derived via the electron affinity rule.

## IV. RESULTS AND DISCUSSION

### A. Electronic structure and branch-point energy of TCOs

The computed gap energies  $E_g$  in Table II agree well with values measured for the TCOs<sup>19,52,80</sup> with an accuracy of 0.2 eV or better. However, one has to keep in mind that the experimental gap energies are still under discussion. This holds especially for In<sub>2</sub>O<sub>3</sub> for which the values in Ref. 19 are much below the values generally given in the literature (see, e.g., Ref. 2).

For illustration the QP band structures of  $rh$ -In<sub>2</sub>O<sub>3</sub>,  $rt$ -SnO<sub>2</sub>, and  $wz$ -ZnO<sup>18,20,42</sup> are plotted in Fig. 3. The branch-point energies  $E_{BP}$  are shown as well. For all three TCOs they lie within the lowest conduction band near the CBM. The reason is the strong  $\mathbf{k}$  dispersion of the lowest conduction band, which gives rise to an extremely low density of states near the pronounced CBM and relatively large electron affinities (see vacuum level in Fig. 3) in all TCOs. Consequently, surface electron accumulation is found experimentally.<sup>19,35,36</sup> Also the hydrogen level  $H(+/-)$ , which may be identified with the position of the charge-neutrality level is above the CBM. For SnO<sub>2</sub> our results for  $E_{BP}$  are confirmed by other calculations.<sup>81</sup>

Recently, Mönch<sup>82</sup> extracted branch-point energies from measured Schottky barriers. He stated excellent agreement between the results of our procedure with experimental values for group III nitrides but found a slight overestimation of  $E_{BP}$  in the case of In<sub>2</sub>O<sub>3</sub> and ZnO.

The results for  $E_{BP}$  are listed and compared with experimental data in Table II. The measurements of surface electron accumulation for undoped In<sub>2</sub>O<sub>3</sub> and doped samples indicate values of  $E_{BP} = 3.5$ – $3.6$  eV for the In<sub>2</sub>O<sub>3</sub> polymorphs<sup>19,35</sup> in excellent agreement with the theoretical predictions.

In the case of  $wz$ -ZnO the Fermi-level stabilization energy lies 0.2 eV below the CBM.<sup>22</sup> An experimental value of  $E_{BP} = 3.04$  eV extracted from valence-band discontinuities to other semiconductors<sup>83</sup> is also somewhat smaller than the computed one. However, from the knowledge of ZnO-AlN valence-band offsets<sup>84</sup> and that of the branch points in group-III nitrides a characteristic energy  $E_{BP} = 3.78$  eV is derived for ZnO.<sup>36</sup> Surface electron accumulation is also indicated by other measurements,<sup>85</sup> in accordance with our predictions.

Clear experimental data are not available for SnO<sub>2</sub>. However, there is also experimental support for a branch-point energy  $E_{BP}$  lying above the CBM.<sup>36</sup> Agreement with other calculations<sup>81</sup> can be stated.

### B. Ionization potential and electron affinity

The planar-averaged electrostatic potentials near the surface of the studied TCOs are plotted in Fig. 4 for different polymorphs (In<sub>2</sub>O<sub>3</sub>) or different orientations (SnO<sub>2</sub>). They clearly show the surface barrier for electrons and the position of the vacuum level. The positions of the QP conduction and valence-band edges,  $E_c$  and  $E_v$ , are also given.

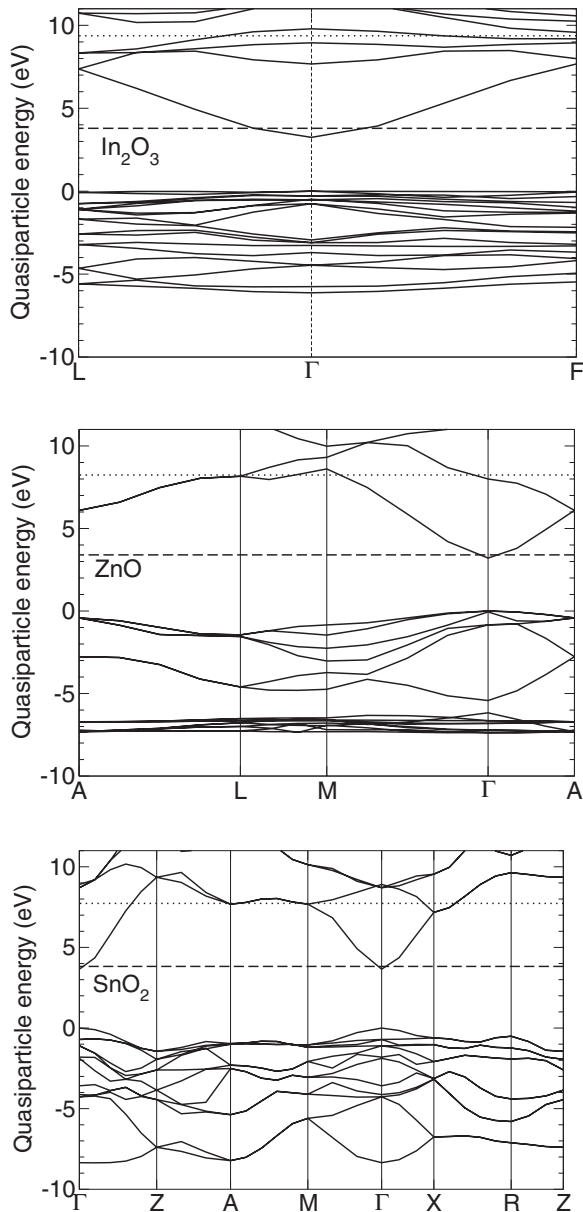


FIG. 3. QP band structures of  $rh$ - $\text{In}_2\text{O}_3$ ,<sup>18</sup>  $wz$ - $\text{ZnO}$ ,<sup>42</sup> and  $rt$ - $\text{SnO}_2$ .<sup>20</sup> The top of the valence bands is used as energy zero. The dashed-dotted lines indicate the branch-point energy-vacuum level.

The surface properties of  $\text{In}_2\text{O}_3$  and Sn-doped  $\text{In}_2\text{O}_3$  [indium-tin oxide (ITO)] are poorly known. Depending on the doping concentration the electron affinity seems to vary in the range of  $A = 4.1$ – $5.0$  eV (see Ref. 17 and references therein). Together with a previously adopted gap of 3.6 eV, ionization energies of  $I = 7.7$ – $8.6$  eV may be derived. Klein<sup>21</sup> suggested values of  $A = 3.5 \pm 0.2$  eV and  $I = 7.1 \pm 0.15$  eV for evaporated  $\text{In}_2\text{O}_3$  films. In a more recent paper<sup>26</sup> the same author gave values of  $A = 4.45$  eV and  $I = 8.05$  eV for ITO samples. Our theoretical values seem to overestimate the experimental findings. The discrepancies to the largest experimental values are of the order of 0.5 eV. As mentioned above, one reason could be the neglect of vertex corrections in the  $GW$  approximation. Apart from uncertainties in the theoretical description, several problems of the real-structure

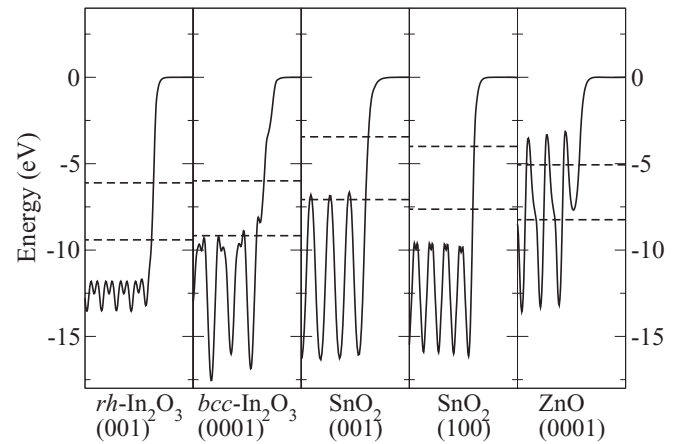


FIG. 4. Planar-averaged electrostatic potential (solid line) near the surface for  $bcc$ - $\text{In}_2\text{O}_3(001)$ ,  $rh$ - $\text{In}_2\text{O}_3(0001)$ ,  $rt$ - $\text{SnO}_2(001)$ ,  $rt$ - $\text{SnO}_2(100)$ , and  $wz$ - $\text{ZnO}(0001)$  as computed within DFT. The QP levels  $E_c$  and  $E_v$  are indicated by dashed horizontal lines. The vacuum level is used as zero of energy.

surfaces such as doping influence, coverage (and hence surface dipole), and sample quality may occur. Also the gap value of 3.6 eV taken from optical measurements deviates by 0.5 eV from the recently predicted one,<sup>19</sup> mostly due to the fact that the lowest interband transitions are dipole forbidden in the bixbyite structure.<sup>86</sup>

In the case of  $wz$ - $\text{ZnO}$ , there is a wide range of measured values. Jacobi *et al.*<sup>87</sup> found electron affinities of  $A = 3.7$ , 4.5, and 4.6 eV in dependence of the surface orientation and termination. Another electrically measured electron affinity amounts to  $A = 4.64$  eV.<sup>89</sup> A value of  $A = 4.05$  eV is derived from studies of the semiconductor-electrolyte interface,<sup>88</sup> which yields  $I = 7.45$  eV taking into account the known gap.<sup>23</sup> Another measurement gave  $I = 7.82$  eV.<sup>16</sup> All in all, these experimental values are close to our theoretical prediction and calculated values from the literature.<sup>90</sup>

Knowledge of the surface properties of  $\text{SnO}_2$  is poorer. Measurements gave  $A = 4.44$  eV<sup>88</sup> which, in combination with the gap of 3.6 eV measured for  $rt$ - $\text{SnO}_2$ ,<sup>23</sup> yields an ionization energy of  $I = 8.04$  eV. In the case of tetragonal  $\text{SnO}_2$ , sometimes doped with Sb, a variation in the interval  $I = 7.9$ – $8.9$  eV is reported.<sup>37</sup>  $\text{SnO}_2$  is therefore the only TCO where our predictions seem to underestimate the experimental value. This might be connected with a possible influence of ViGS at this surface (see below).

The experimental ionization energy of Si lies in the interval  $I = 5.15$ – $5.33$  eV for different orientations and reconstructions.<sup>16</sup> These values lead to  $A = 4.0$ – $4.2$  eV taking the Si gap value into account. Our values calculated within the HSE+ $G_0W_0$  framework seem to indicate a slight underestimation of  $I$  and  $A$  by about 0.3 eV. One reason could be dipole effects that are not included in the QP approach.

### C. Band discontinuities for Si-TCO heterojunctions

The branch-point energies  $E_{BP}$  as well as the electron affinities  $A$  and the ionization potentials  $I$  in Table II are used to compute two types of natural-band discontinuities

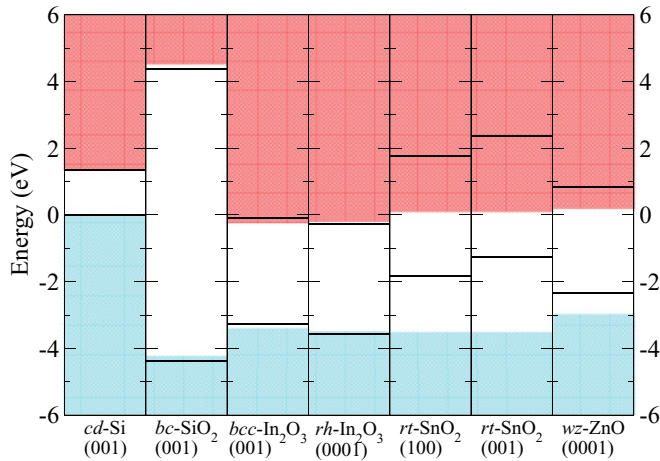


FIG. 5. (Color online) Conduction-band and valence-band edges for silicon, SiO<sub>2</sub>, In<sub>2</sub>O<sub>3</sub>, SnO<sub>2</sub>, and ZnO. Different universal levels are used for the band alignment: The blue and red colored areas show the valence and conduction bands, respectively, in the alignment via the branch-point energy  $E_{BP}$ . The horizontal lines show the alignment via the vacuum level  $E_{vac}$ . The calculated energies from Tables II and III have been applied. The silicon VBM is used as zero of energy.

$\Delta E_c$  and  $\Delta E_v$  (see Sec. III B and III C). The resulting band offsets are listed in Table III and the band lineup is shown in Fig. 5. In the case of the alignment via the branch-point energies  $E_{BP}$  as reference level only the Si-SiO<sub>2</sub> interface represents a type-I heterostructure. For the Si-TCO interfaces we observe  $\Delta E_c < 0$  and, hence, staggered type-II heterojunctions.<sup>14</sup> In the case of the Si-In<sub>2</sub>O<sub>3</sub> interfaces we see  $|\Delta E_c| > E_g(\text{Si})$ . Therefore, these structures even represent a misaligned type-III heterostructure<sup>14</sup> sometimes also called broken-gap heterostructure.<sup>91</sup> Since this would imply that the lowest conduction-band states on the oxide side of the interface are energetically favored over the valence-band states in the silicon, we predict a charge transfer upon interface formation that should alter the interface dipole and shift the band edges toward a stable type-II junction.

For the band offsets obtained by using the vacuum level  $E_{vac}$  as reference energy, the qualitative behavior is (cf. Fig. 5) largely conserved. The only qualitative change between the two alignment procedures occurs for the heterojunction Si-SnO<sub>2</sub>. In contrast to the  $E_{BP}$  alignment the vacuum-level alignment yields a type-I heterostructure. There are several possible reasons for this discrepancy. One is that the Tersoff method<sup>32</sup> does not take into account electrostatic effects occurring at surfaces and interfaces. The existence of surface dipole moments can have a strong influence on the values of  $I$  and  $A$  and, hence, the band alignment, especially for polar materials with ionic bonds. Since a real interface would inevitably possess an interface dipole, it is clear that the band discontinuities of Si-TCO heterostructures strongly depend on the surface orientation and the interface structure. Mönch<sup>25</sup> stated that the electric-dipole contribution can change the valence-band offsets in semiconductor heterostructures by up to 30%.

In order to investigate the influence of such a dipole, we have calculated  $I$  and  $A$  for  $rt$ -SnO<sub>2</sub> for two different

orientations, the nonpolar (001) direction and the polar (100) direction. The values in Table II clearly indicate a significant variation of the surface barrier with the surface orientation and termination. Yet both orientations show the tendency for the formation of a type-I heterostructure for Si- $rt$ -SnO<sub>2</sub> interfaces as indicated by the positive band discontinuities  $\Delta E_c$  and  $\Delta E_v$  in Table III. The variations of  $I$  and  $A$  with the surface orientation, though considerable, are not sufficient to explain the different sets of band offsets for these two materials. Another possible reason is that interface states located in the fundamental gap might play a very important role for the Si-SnO<sub>2</sub> interface. As a consequence the electron-affinity rule would fail. Further investigations of SnO<sub>2</sub> surfaces and their interfaces with Si should be carried out in order to clarify the discrepancy.

Experimental values for the band discontinuities are rather rare. In the case of the Si-In<sub>2</sub>O<sub>3</sub> heterojunction the corresponding barrier  $\Delta E_c = -0.61$  eV for electrons going from In<sub>2</sub>O<sub>3</sub> to Si has recently been measured by means of photoinjection.<sup>92</sup> Together with the bulk gaps  $E_g = 3.1$  eV (from optical absorption of In<sub>2</sub>O<sub>3</sub>) and  $E_g = 1.1$  eV (for Si) a valence-band discontinuity of  $\Delta E_v = 2.6$  eV is derived. The combination of measured valence-band discontinuities  $\Delta E_v = 2.1$  eV for CdTe-In<sub>2</sub>O<sub>3</sub> heterojunctions<sup>93</sup> and  $\Delta E_v = 0.75$  eV for Si-CdTe<sup>94,95</sup> suggests a value  $\Delta E_v = 2.85$  eV for Si-In<sub>2</sub>O<sub>3</sub> junctions applying the transitivity rule.<sup>14</sup> Together with the gap difference of about  $\Delta E_g = 2.0$  eV a conduction-band discontinuity of about  $\Delta E_c = -0.85$  eV may be derived. Both the type of the heterostructure (i.e., the signs of  $\Delta E_c$  and  $\Delta E_v$ ) and the order of magnitude are in agreement with our predictions using two different band alignments (cf. Table III).

For the Si-ZnO interface band offsets  $\Delta E_c = -0.4$  eV and  $\Delta E_v = 2.55$  eV have been estimated from measured electron affinities and/or work functions of  $p$ -Si and  $n$ -ZnO.<sup>12</sup> From electrical measurements electron barriers of  $\Delta E_c = -0.45$  ( $n$ -Si) or  $\Delta E_c = -0.69$  or  $-0.72$  eV ( $p$ -Si) have been derived,<sup>11</sup> which indicate an influence of the doping level. In addition, there is a value  $\Delta E_v = 2.7$  eV for Ge-ZnO.<sup>96</sup> Together with  $\Delta E_v = -0.17$  eV for Si-Ge<sup>94,95</sup> we can calculate an offset  $\Delta E_v = 2.53$  eV for Si-ZnO, using the transitivity rule. Employing the gap difference  $\Delta E_g = 2.3$  eV one derives  $\Delta E_c = -0.23$  eV. All these values are in agreement with our prediction of a type-II heterostructure.

Little is known about the electronic properties of the Si-SnO<sub>2</sub> interface. Only indirect information is available. The valence-band discontinuity for CdS-SnO<sub>2</sub> amounts to  $\Delta E_v = 1.2 \pm 0.2$  eV.<sup>97</sup> Together with the value  $\Delta E_v = 1.55$  eV for Si-CdS interface<sup>94,95</sup> one obtains  $\Delta E_v = 2.75$  eV for Si-SnO<sub>2</sub> junction applying the transitivity rule.<sup>14</sup> With the gap difference  $\Delta E_g = 2.5$  eV a conduction-band offset  $\Delta E_c = -0.25$  eV can be derived. While this prediction is in agreement with the alignment via  $E_{BP}$  with regard to the type of the junction, it actually falls halfway between the two contradicting sets of band offsets derived via the two different alignment methods, so that it cannot really serve as an indicator, which of this two methods gives the better result for the band discontinuities.

All in all, the experimental data also indicate a misaligned type-II heterocharacter of the Si-TCO interfaces, in agreement with our predictions.

## V. CONCLUSION

Modern quasiparticle theory has been applied to the transparent conducting oxides  $\text{In}_2\text{O}_3$ ,  $\text{ZnO}$ , and  $\text{SnO}_2$ . The resulting band structures with rather accurate fundamental energy gaps were used to compute the branch-point energies for the Si as well as, for the purpose of comparison, for  $\text{SiO}_2$ . A combination with surface calculations allows the derivation of electron affinities and ionization energies (i.e., the absolute positions of the conduction-band minima and valence-band maxima with respect to the vacuum level). For this, the bulk and surface electronic structures have been aligned by means of the electrostatic potentials.

The results were used to derive conduction-band and valence-band offsets for heterostructures of silicon with the oxides. The alignment of the electronic structures across the heterojunction was made using both the branch-point energies and the vacuum levels, resulting in two different sets of natural-band offsets. The obtained values have been compared and discussed in the light of the limited experimental data available.

The two alignment methods give almost the same results for the benchmark Si- $\text{SiO}_2$  interface. It represents a type-I

heterostructure with relatively large band offsets  $\Delta E_c$  and  $\Delta E_v$ . The application of both alignment methods yields type-II heterojunctions for the Si- $\text{In}_2\text{O}_3$  and Si- $\text{ZnO}$  interfaces. In the  $\text{In}_2\text{O}_3$  case even a tendency to a type-III heterostructure is visible. Only in the case of the Si- $\text{SnO}_2$  interface the alignments via  $E_{\text{BP}}$  and  $E_{\text{vac}}$  give rise to qualitatively opposite results, a type-II or a type-I heterostructure, respectively. The type-II behavior seems to be in agreement with experimental indications. We conclude that for this heterojunction electronic states in the fundamental gaps play an important role.

## ACKNOWLEDGMENTS

The authors are grateful to F. Fuchs, T. D. Veal, P. D. C. King, and M. Schmidt for valuable discussions. We acknowledge support from the German Federal Government (BMBF Projects No. 13N9669 and No. 03SF0308), the Carl-Zeiss-Stiftung, the Deutsche Forschungsgemeinschaft (Project No. Be1346/20-1), and the European Community in the framework of ETSF (GA No. 211956). Further, we thank the LRZ Munich and HLRZ Stuttgart for computing time.

\*benjamin.hoeffling@uni-jena.de

<sup>1</sup>D. S. Ginley and C. G. E. Bright, *MRS Bull.* **25**, 15 (2000).

<sup>2</sup>Z. M. Jarzelski, *Phys. Status Solidi A* **71**, 13 (1982).

<sup>3</sup>Y. Li, G. S. Tompa, S. Liang, C. Gorla, Y. Lu, and J. Doyle, *Transparent and Conductive Ga-doped ZnO Films Grown by Low Pressure Metal Organic Chemical Vapor Deposition* (AVS, Philadelphia, 1997), No. 3, pp. 1063–1068.

<sup>4</sup>P. P. Edwards, A. Porch, M. O. Jones, D. V. Morgan, and R. M. Perks, *Dalton Trans.* 2995 (2004).

<sup>5</sup>G. Thomas, *Nature (London)* **389**, 907 (1997).

<sup>6</sup>K. Nomura, H. Ohta, K. Ueda, T. Kamiya, M. Hirano, and H. Hosono, *Science* **300**, 1269 (2003).

<sup>7</sup>R. W. Miles, G. Zoppi, and I. Forbes, *Mater. Today* **10**, 20 (2007).

<sup>8</sup>X. Zhang, Q. Zhang, and F. Lu, *Semicond. Sci. Technol.* **22**, 900 (2007).

<sup>9</sup>Z.-X. Fu, B.-X. Lin, and G.-H. Liao, *Chin. Phys. Lett.* **16**, 753 (1999).

<sup>10</sup>S. M. Sze, *Physics of Semiconductor Devices*, 2nd ed. (Wiley, New York, 1981).

<sup>11</sup>K. B. Sundaram and A. Khan, *J. Vac. Sci. Technol. A* **15**, 428 (1997).

<sup>12</sup>I.-S. Jeong, J. H. Kim, and S. Im, *Appl. Phys. Lett.* **83**, 2946 (2003).

<sup>13</sup>E. H. Rhoderick, *Metal-Semiconductor Contacts* (Clarendon Press, Oxford, 1978).

<sup>14</sup>F. Bechstedt and R. Enderlein, *Semiconductor Surfaces and Interfaces* (Akademie-Verlag, Berlin, 1988).

<sup>15</sup>R. Anderson, *Solid-State Electron.* **5**, 341 (1962).

<sup>16</sup>W. Mönch, *Semiconductor Surfaces and Interfaces* (Springer, Berlin, 2001).

<sup>17</sup>A. Klein, C. Körber, A. Wachau, F. Säuberlich, Y. Gassenbauer, R. Schafranek, S. Harvey, and T. Mason, *Thin Solid Films* **518**, 1197 (2009).

<sup>18</sup>F. Fuchs and F. Bechstedt, *Phys. Rev. B* **77**, 155107 (2008).

<sup>19</sup>P. D. C. King *et al.*, *Phys. Rev. B* **79**, 205211 (2009).

<sup>20</sup>A. Schleife, J. B. Varley, F. Fuchs, C. Rödl, F. Bechstedt, P. Rinke, A. Janotti, and C. G. Van de Walle, *Phys. Rev. B* **83**, 035116 (2011).

<sup>21</sup>A. Klein, *Appl. Phys. Lett.* **77**, 2009 (2000).

<sup>22</sup>W. Walukiewicz, *Physica B* **302-303**, 123 (2001).

<sup>23</sup>C. Kilic and A. Zunger, *Appl. Phys. Lett.* **81**, 73 (2002).

<sup>24</sup>S. Harvey, T. Mason, Y. Gassenbauer, R. Schafranek, and A. Klein, *J. Phys. D: Appl. Phys.* **39**, 3959 (2006).

<sup>25</sup>W. Mönch, *Appl. Phys. Lett.* **93**, 172118 (2008).

<sup>26</sup>Y. Gassenbauer and A. Klein, *J. Phys. Chem. B* **110**, 4793 (2006).

<sup>27</sup>W. R. Frensley and H. Kroemer, *J. Vac. Sci. Technol.* **13**, 810 (1976).

<sup>28</sup>V. Heine, *Phys. Rev. A* **138**, 1689 (1965).

<sup>29</sup>S. G. Louie and M. L. Cohen, *Phys. Rev. B* **13**, 2461 (1976).

<sup>30</sup>F. Flores and C. Tejedor, *J. Phys. C Solid State* **12**, 731 (1979).

<sup>31</sup>W. Mönch, *Electronic Properties of Semiconductor Interfaces* (Springer, Berlin, 2004).

<sup>32</sup>J. Tersoff, *Phys. Rev. B* **30**, 4874 (1984).

<sup>33</sup>C. Tejedor and F. Flores, *J. Phys. C* **11**, L19 (1977).

<sup>34</sup>A. Schleife, F. Fuchs, C. Rödl, J. Furthmüller, and F. Bechstedt, *Appl. Phys. Lett.* **94**, 012104 (2009).

<sup>35</sup>P. D. C. King, T. D. Veal, D. J. Payne, A. Bourlange, R. G. Egdell, and C. F. McConville, *Phys. Rev. Lett.* **101**, 116808 (2008).

<sup>36</sup>P. D. C. King *et al.*, *Phys. Rev. B* **80**, 081201 (2009).

<sup>37</sup>C. Körber, P. Agoston, and A. Klein, *Sensors and Actuators B* **139**, 665 (2009).

<sup>38</sup>B. Höffling, A. Schleife, F. Fuchs, C. Rödl, and F. Bechstedt, *Appl. Phys. Lett.* **97**, 032116 (2010).

<sup>39</sup>W. R. L. Lambrecht and B. Segall, *Phys. Rev. Lett.* **61**, 1764 (1988).

<sup>40</sup>W. R. L. Lambrecht, B. Segall, and O. K. Andersen, *Phys. Rev. B* **41**, 2813 (1990).

- <sup>41</sup>F. Fuchs, J. Furthmüller, F. Bechstedt, M. Shishkin, and G. Kresse, *Phys. Rev. B* **76**, 115109 (2007).
- <sup>42</sup>A. Schleife, C. Rödl, F. Fuchs, J. Furthmüller, and F. Bechstedt, *Phys. Rev. B* **80**, 035112 (2009).
- <sup>43</sup>A. R. H. Preston, B. J. Ruck, L. F. J. Piper, A. DeMasi, K. E. Smith, A. Schleife, F. Fuchs, F. Bechstedt, J. Chai, and S. M. Durbin, *Phys. Rev. B* **78**, 155114 (2008).
- <sup>44</sup>P. Hohenberg and W. Kohn, *Phys. Rev. B* **136**, 864 (1964).
- <sup>45</sup>W. Kohn and L. J. Sham, *Phys. Rev. A* **140**, 1133 (1965).
- <sup>46</sup>D. M. Ceperley and B. J. Alder, *Phys. Rev. Lett.* **45**, 566 (1980).
- <sup>47</sup>J. P. Perdew, in *Electronic Structure of Solids '91* (Akademie-Verlag, Berlin, 1991), p. 11.
- <sup>48</sup>G. Kresse and J. Furthmüller, *Comput. Mater. Sci.* **6**, 15 (1996).
- <sup>49</sup>G. Kresse and D. Joubert, *Phys. Rev. B* **59**, 1758 (1999).
- <sup>50</sup>K. Seino, J.-M. Wagner, and F. Bechstedt, *Appl. Surf. Sci.* **255**, 787 (2008).
- <sup>51</sup>H. J. Monkhorst and J. D. Pack, *Phys. Rev. B* **13**, 5188 (1976).
- <sup>52</sup>*Springer Handbook of Condensed Matter and Materials Data*, edited by W. Martienssen and H. Warlimont (Springer, Berlin, 2005), p. 660.
- <sup>53</sup>T. Demuth, Y. Jeanvoine, J. Hafner, and J. G. Angyan, *J. Phys. Condens. Matter* **11**, 3833 (1999).
- <sup>54</sup>*ICSD, Inorganics Crystal Structure Database* (Fachinformationzentrum Karlsruhe, Germany, 2002).
- <sup>55</sup>J. Haines and J. M. Léger, *Phys. Rev. B* **55**, 11144 (1997).
- <sup>56</sup>L. E. Ramos, J. Furthmüller, and F. Bechstedt, *Phys. Rev. B* **69**, 085102 (2004).
- <sup>57</sup>A. Schleife, F. Fuchs, J. Furthmüller, and F. Bechstedt, *Phys. Rev. B* **73**, 245212 (2006).
- <sup>58</sup>F. Bechstedt, F. Fuchs, and G. Kresse, *Phys. Status Solidi B* **246**, 1877 (2009).
- <sup>59</sup>J. Heyd, G. E. Scuseria, and M. Ernzerhof, *J. Chem. Phys.* **118**, 8207 (2003).
- <sup>60</sup>J. Heyd, G. E. Scuseria, and M. Ernzerhof, *J. Chem. Phys.* **124**, 219906 (2006).
- <sup>61</sup>A. V. Krukau, O. A. Vydrov, A. F. Izmaylov, and G. E. Scuseria, *J. Chem. Phys.* **125**, 224106 (2006).
- <sup>62</sup>J. Paier, M. Marsman, K. Hummer, G. Kresse, I. C. Gerber, and J. G. Ángyán, *J. Chem. Phys.* **124**, 154709 (2006).
- <sup>63</sup>J. Paier, M. Marsman, K. Hummer, G. Kresse, I. C. Gerber, and J. G. Ángyán, *J. Chem. Phys.* **125**, 249901 (2006).
- <sup>64</sup>M. Shishkin and G. Kresse, *Phys. Rev. B* **74**, 035101 (2006).
- <sup>65</sup>A. Schleife *et al.*, *J. Korean Phys. Soc.* **53**, 2811 (2008).
- <sup>66</sup>C. G. Van de Walle and R. M. Martin, *Phys. Rev. B* **34**, 5621 (1986).
- <sup>67</sup>D. M. Bylander and L. Kleinman, *Phys. Rev. B* **36**, 3229 (1987).
- <sup>68</sup>K. Seino, J.-M. Wagner, and F. Bechstedt, *Appl. Phys. Lett.* **90**, 253109 (2007).
- <sup>69</sup>J. Tersoff, *Phys. Rev. B* **32**, 6968 (1985).
- <sup>70</sup>M. Cardona and N. E. Christensen, *Phys. Rev. B* **35**, 6182 (1987).
- <sup>71</sup>C. G. Van de Walle and J. Neugebauer, *Nature (London)* **423**, 626 (2003).
- <sup>72</sup>S.-H. Wei and A. Zunger, *Appl. Phys. Lett.* **72**, 2011 (1998).
- <sup>73</sup>W. Aulbur, L. Jönsson, and J. Wilkins, in *Solid State Physics: Advances in Research and Applications*, edited by H. Ehrenreich and F. Spaepen (Academic Press, New York, 2000), Vol. 54, p. 1.
- <sup>74</sup>A. G. Milnes and D. L. Feucht, *Heterojunctions and Metal-Semiconductor Junctions* (Academic Press, New York, 1972).
- <sup>75</sup>R. Del Sole, L. Reining, and R. W. Godby, *Phys. Rev. B* **49**, 8024 (1994).
- <sup>76</sup>R. Shaltaf, G.-M. Rignanese, X. Gonze, F. Giustino, and A. Pasquarello, *Phys. Rev. Lett.* **100**, 186401 (2008).
- <sup>77</sup>Z. A. Weinberg, G. W. Rubloff, and E. Bassous, *Phys. Rev. B* **19**, 3107 (1979).
- <sup>78</sup>A. Alkauskas, P. Broqvist, F. Devynck, and A. Pasquarello, *Phys. Rev. Lett.* **101**, 106802 (2008).
- <sup>79</sup>C. Sgaravello, N. Binggeli, and A. Baldereschi, *Phys. Rev. B* **64**, 195305 (2001).
- <sup>80</sup>K. Reimann and M. Steube, *Solid State Commun.* **105**, 649 (1998).
- <sup>81</sup>B. Falabretti and J. Robertson, *J. Appl. Phys.* **102**, 123703 (2007).
- <sup>82</sup>W. Mönch, *J. Appl. Phys.* **109**, 113724 (2011).
- <sup>83</sup>W. Mönch, *Appl. Phys. Lett.* **86**, 162101 (2005).
- <sup>84</sup>T. D. Veal, P. D. C. King, S. A. Hatfield, L. R. Bailey, C. F. McConville, B. Martel, J. C. Moreno, E. Frayssinet, F. Semond, and J. Zúñiga-Pérez, *Appl. Phys. Lett.* **93**, 202108 (2008).
- <sup>85</sup>M. W. Allen, C. H. Swartz, T. H. Myers, T. D. Veal, C. F. McConville, and S. M. Durbin, *Phys. Rev. B* **81**, 075211 (2010).
- <sup>86</sup>A. Walsh *et al.*, *Phys. Rev. Lett.* **100**, 167402 (2008).
- <sup>87</sup>K. Jacobi, G. Zwicker, and A. Gutmann, *Surf. Sci.* **141**, 109 (1984).
- <sup>88</sup>M. A. Butler and D. S. Ginley, *J. Electrochem. Soc.* **125**, 228 (1978).
- <sup>89</sup>W. Göpel, L. J. Brillson, and C. F. Brucker, *J. Vac. Sci. Technol.* **17**, 894 (1980).
- <sup>90</sup>D. Vogel, Ph.D. thesis, Universität Münster, 1998.
- <sup>91</sup>C. Kittel, *Introduction to Solid State Physics*, 8th ed. (Wiley, New York, 2005).
- <sup>92</sup>M. Schmidt, H. Angermann, E. Conrad, L. Korte, A. Laades, K. von Maydell, D. Schaffarzik, A. Schöpke, C. Schubert, and R. Stangl, *Grundlagen und Technologie von Solarzellen auf der Basis von a-Si/c-Si-Heterostrukturen* (Mensch & Buch Verlag, Berlin, 2007).
- <sup>93</sup>F. Rüggeberg and A. Klein, *Appl. Phys. A* **82**, 281 (2006).
- <sup>94</sup>A. D. Katnani and G. Margaritondo, *Phys. Rev. B* **28**, 1944 (1983).
- <sup>95</sup>G. Margaritondo, *Phys. Rev. B* **31**, 2526 (1985).
- <sup>96</sup>M. Ruckh, D. Schmid, and H. W. Schock, *J. Appl. Phys.* **76**, 5945 (1994).
- <sup>97</sup>J. Fritsche, D. Kraft, A. Thißen, T. Mayer, A. Klein, and W. Jaegermann, *Thin Solid Films* **403-404**, 252 (2002).